Studies of azimuthal anisotropy harmonics in ultra-central PbPb collisions at sqrt(s[NN]) = 2.76 TeV

CMS Collaboration ; Chatrchyan, S ; Khachatryan, V ; Sirunyan, A M ; et al ; Chiochia, V ; Kilminster, B ; Robmann, P

Abstract: Azimuthal dihadron correlations of charged particles have been measured in PbPb collisions at sqrt(s[NN]) = 2.76 TeV by the CMS collaboration, using data from the 2011 LHC heavy-ion run. The data set includes a sample of ultra-central (0-0.2% centrality) PbPb events collected using a trigger based on total transverse energy in the hadron forward calorimeters and the total multiplicity of pixel clusters in the silicon pixel tracker. A total of about 1.8 million ultra-central events were recorded, corresponding to an integrated luminosity of 120 inverse microbarns. The observed correlations in ultra-central PbPb events are expected to be particularly sensitive to initial-state fluctuations. The single-particle anisotropy Fourier harmonics, from v[2] to v[6], are extracted as a function of particle transverse momentum. At higher transverse momentum, the v[2] harmonic becomes significantly smaller than the higher-order v[n] (n greater than or equal to 3). The pt-averaged v[2] and v[3] are found to be equal within 2%, while higher-order v[n] decrease as n increases. The breakdown of factorization of dihadron correlations into single-particle azimuthal anisotropies is observed. This effect is found to be most prominent in the ultra-central PbPb collisions, where the initial-state fluctuations play a dominant role. A comparison of the factorization data to hydrodynamic predictions with event-by-event fluctuating initial conditions is also presented.

DOI: https://doi.org/10.1007/JHEP02(2014)088

EUROPEAN ORGANIZATION FOR NUCLEAR RESEARCH (CERN)

CERN-PH-EP/2013-221
2013/12/09

CMS-HIN-12-011

Studies of azimuthal dihadron correlations in ultra-central PbPb collisions at $\sqrt{s_{NN}} = 2.76$ TeV

The CMS Collaboration

Abstract

Azimuthal dihadron correlations of charged particles have been measured in PbPb collisions at $\sqrt{s_{NN}} = 2.76$ TeV by the CMS collaboration, using data from the 2011 LHC heavy-ion run. The data set includes a sample of ultra-central (0–0.2% centrality) PbPb events collected using a trigger based on total transverse energy in the hadron forward calorimeters and the total multiplicity of pixel clusters in the silicon pixel tracker. A total of about 1.8 million ultra-central events were recorded, corresponding to an integrated luminosity of 120 μb^{-1}. The observed correlations in ultra-central PbPb events are expected to be particularly sensitive to initial-state fluctuations. The single-particle anisotropy Fourier harmonics, from v_2 to v_6, are extracted as a function of particle transverse momentum. At higher transverse momentum, the v_2 harmonic becomes significantly smaller than the higher-order v_n ($n \geq 3$). The p_{T}-averaged v_2 and v_3 are found to be equal within 2%, while higher-order v_n decrease as n increases. The breakdown of factorization of dihadron correlations into single-particle azimuthal anisotropies is observed. This effect is found to be most prominent in the ultra-central PbPb collisions, where the initial-state fluctuations play a dominant role. A comparison of the factorization data to hydrodynamic predictions with event-by-event fluctuating initial conditions is also presented.

Submitted to the Journal of High Energy Physics

1 Introduction

The azimuthal anisotropy of emitted charged particles is an important feature of the hot, dense medium produced in heavy-ion collisions. One of the main goals of studying the azimuthal anisotropies is to understand the collective properties of the medium and extract its transport coefficients, particularly the shear viscosity over entropy density ratio, η/s, using hydrodynamic models [1]. Earlier observations of strong azimuthal anisotropies in collisions of gold nuclei at nucleon-nucleon center-of-mass energies ($\sqrt{s_{NN}}$) up to 200 GeV at the Relativistic Heavy-Ion Collider (RHIC) indicated that a strongly coupled quark-gluon plasma is produced, which behaves as a nearly perfect liquid with a close-to-zero η/s value [2–7]. The azimuthal anisotropies have also been extensively measured at the Large Hadron Collider (LHC) over a wide kinematic range in PbPb collisions at $\sqrt{s_{NN}}$ = 2.76 TeV [8–17].

In a non-central heavy-ion collision, the overlap region of the two colliding nuclei has a lenticular shape, and the interacting nucleons in this region are known as "participants." The "participant plane" is defined by the beam direction and the short axis of the participating nucleon distribution. Because of fluctuations that arise from the finite number of nucleons, the impact parameter vector typically does not coincide with the short axis of this lenticular region. Strong rescattering of the partons in the initial state may lead to local thermal equilibrium and the build-up of anisotropic pressure gradients, which drive a collective anisotropic expansion. The expansion is fastest along the largest pressure gradient, i.e., along the short axis of the lenticular region. Therefore, the eccentricity of initial-state collision geometry results in an anisotropic azimuthal distribution of the final-state hadrons. In general, the anisotropy can be characterized by the Fourier harmonic coefficient (v_n) in the azimuthal angle (ϕ) distribution of the hadron yield, $\mathrm{d}N/\mathrm{d}\phi \propto 1 + 2\sum_n v_n \cos[n(\phi - \Psi_\mathrm{n})]$, where Ψ_n is the event-by-event azimuthal angle of the participant plane. As the participant plane is not a measurable quantity experimentally, it is often approximated by the "event plane", defined as the direction of maximum final-state particle density. The second-order Fourier component (v_2) is known as the "elliptic flow", and its event plane angle Ψ_2 approximately corresponds to the short axis direction of the lenticular region. Due to event-by-event fluctuations, higher-order deformations or eccentricities of the initial geometry can also be induced, which lead to higher-order Fourier harmonics (v_n, $n \geq 3$) in the final state with respect to their corresponding event plane angles, Ψ_n [18–24]. For a given initial-state eccentricity, the finite η/s value of the system tends to reduce the azimuthal anisotropy observed for final-state particles. The higher-order Fourier harmonics are expected to be particularly sensitive to the shear viscosity of the expanding medium.

Precise extraction of η/s from the anisotropy data is crucial for investigating the transport properties of the hot and dense medium created in heavy-ion collisions in detail [1]. This effort is, however, complicated by large uncertainties in our understanding of the initial-state conditions of heavy-ion collisions, especially in terms of event-by-event fluctuations. Different initial-state models predict different values of eccentricity and its fluctuations, leading to large uncertainties on the extracted η/s values. In order to better constrain the initial-state condition, it was suggested [25] that in ultra-central heavy-ion collisions (e.g., top 1% most central collisions), the initial collision geometry is predominantly generated by fluctuations such that various orders of eccentricities predicted by different models tend to converge. Here, collision centrality is defined as the fraction of the total inelastic PbPb cross section, with 0% denoting the most central collisions. Therefore, studies of azimuthal anisotropy in ultra-central heavy-ion collisions can help to reduce the systematic uncertainties of initial-state modeling in extracting the η/s value of the system.

Furthermore, since the event plane angle, Ψ_n, is determined by the final-state particles, select-

ing particles from different ranges of transverse momentum (p_T) may lead to different estimates of event plane angles. Also due to the effect of initial-state fluctuations, it was recently predicted by hydrodynamic models that a p_T-dependence of the event plane angle will be induced, which could be one of the sources responsible for the breakdown of factorization in extracting v_n harmonics from dihadron correlations [26, 27]. As mentioned already, the ultra-central heavy-ion events are dominated by the initial-state eccentricity fluctuations. Thus, they provide an ideal testing ground for the effect of a p_T-dependent event plane angle.

This paper presents the measurement of azimuthal anisotropy harmonics, from v_2 to v_6, extracted using long-range (large $|\Delta\eta|$) dihadron correlations as a function of p_T from 0.3 to 8.0 GeV/c in the top 0.2% most central PbPb collisions at a center-of-mass energy per nucleon pair ($\sqrt{s_{NN}}$) of 2.76 TeV. Here, $\Delta\eta$ is the difference in pseudorapidity $\eta = -\ln[\tan(\theta/2)]$ between the two particles, where the polar angle θ is defined relative to the beam axis. The p_T-averaged v_n values for $0.3 < p_T < 3.0$ GeV/c are also derived up to $n = 7$. Factorization of the Fourier coefficients from dihadron correlations into a product of single-particle azimuthal anisotropies is investigated. This study of factorization is quantitatively compared to hydrodynamic predictions with different models of initial-state fluctuations and η/s values for two centrality classes.

2 Experimental Setup

The data used in this analysis correspond to an integrated luminosity of 120 μb^{-1} and were recorded with the CMS detector during the 2011 PbPb LHC running period at $\sqrt{s_{NN}} = 2.76$ TeV. A detailed description of the CMS detector can be found in Ref. [28]. The CMS uses a right-handed coordinate system, with the origin at the nominal interaction point, the x axis pointing to the centre of the LHC, the y axis pointing up (perpendicular to the LHC plane), and the z axis along the anticlockwise-beam direction. The polar angle θ is measured from the positive z axis and the azimuthal angle (ϕ) is measured in the x-y plane. The central feature of the apparatus is a superconducting solenoid of 6 m internal diameter, providing a magnetic field of 3.8 T. Within the field volume are the silicon pixel and strip trackers, the crystal electromagnetic calorimeter, and the brass/scintillator hadron calorimeter. In PbPb collisions, trajectories of charged particles with $p_T > 0.2$ GeV/c are reconstructed in the tracker covering the pseudorapidity region $|\eta| < 2.5$, with a track momentum resolution of about 1% at $p_T = 100$ GeV/c. In addition, CMS has extensive forward calorimetry, in particular two steel/quartz-fiber Cherenkov hadron forward (HF) calorimeters, which cover the pseudorapidity range $2.9 < |\eta| < 5.2$. The HF calorimeters are segmented into towers, each of which is a two-dimensional cell with a granularity of 0.5 units in η and 0.349 rad in ϕ. The zero-degree calorimeters (ZDC) are tungsten/quartz Cherenkov calorimeters located at $\pm$140 mm from the interaction point [29]. They are designed to measure the energy of photons and spectator neutrons emitted from heavy ion collisions. Each ZDC calorimeter has electromagnetic and hadronic sections with an active area of $\pm$40 mm in x and $\pm$50 mm in y. When the LHC beam crossing angle is 0 degree, this corresponds to an η acceptance that starts at $\eta = 8.3$ and is 100% by $\eta = 8.9$ for $\sqrt{s_{NN}} = 2.76$ TeV. For one neutron, the ZDCs have an energy resolution of 20%. Since each neutron interacts independently, the resolution improves as the square root of the number of neutrons.

3 Selections of Events and Tracks

Minimum bias PbPb events were triggered by coincident signals from both ends of the detector in either the beam scintillator counters (BSC) at $3.23 < |\eta| < 4.65$ or in the HF calorimeters.

Events due to noise, cosmic rays, out-of-time triggers, and beam backgrounds were suppressed by requiring a coincidence of the minimum bias trigger with bunches colliding in the interaction region. The trigger has an efficiency of $(97 \pm 3)\%$ for hadronic inelastic PbPb collisions. In total, about 2% of all minimum bias PbPb events were recorded.

To maximize the event sample for very central PbPb collisions, a dedicated online trigger on the 0–0.2% ultra-central events was implemented by simultaneously requiring the HF energy sum to be greater than 3260 GeV and the pixel cluster multiplicity to be greater than 51400 (which approximately corresponds to 9500 charged particles over 5 units of pseudorapidity). The selected events correspond to the 0.2% most central collisions of the total PbPb inelastic cross section. The correlation between the HF energy sum and pixel cluster multiplicity for minimum bias PbPb collisions at $\sqrt{s_{NN}}$ = 2.76 TeV is shown in Fig. 1. The dashed lines indicate the selections used for the 0–0.2% centrality range. This fractional cross section is determined relative to the standard 0–2.5% centrality selection in PbPb collisions at CMS by selecting on the total energy deposited in the HF calorimeters [8]. The inefficiencies of the minimum bias trigger and event selection for very peripheral events are properly accounted. In a similar way, the 0–0.02% centrality range is also determined by requiring the HF energy sum greater than 3393 GeV and pixel cluster multiplicity greater than 53450 (a subset of 0–0.2% ultra-central events). With this trigger, the ultra-central PbPb event sample is enhanced by a factor of about 40 compared to the minimum bias sample. For purposes of systematic comparisons, other PbPb centrality ranges, corresponding to 40–50%, 0–10%, 2.5–5.0%, 0–2.5% and 0–1%, are studied based on the HF energy sum selection using the minimum bias sample. As a cross-check, the 0–1% centrality range is also studied using combined HF energy sum and pixel cluster multiplicity, similar to the centrality selection of 0–0.2% ultra-central events.

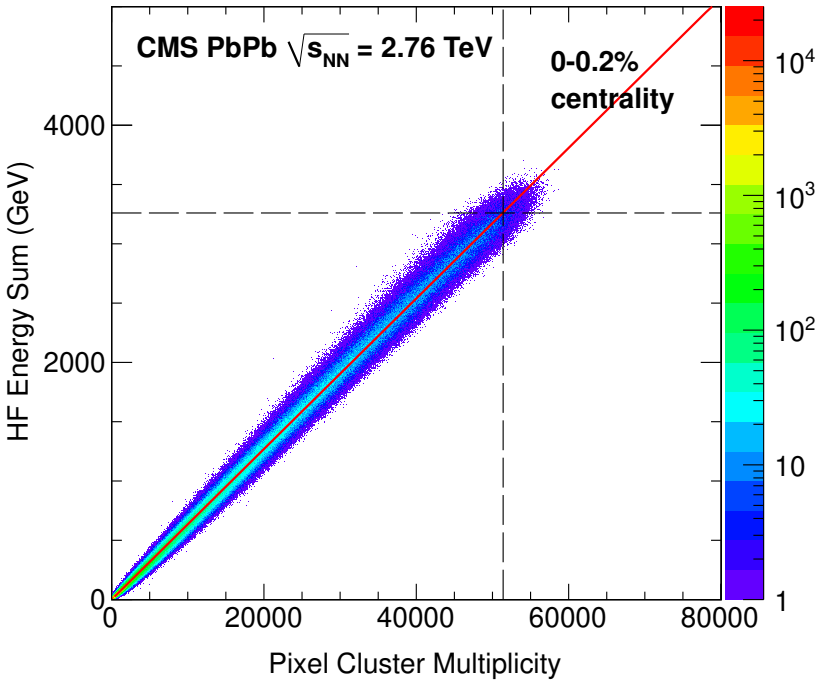

Figure 1: HF energy sum vs. pixel cluster multiplicity for minimum bias triggered PbPb collisions at $\sqrt{s_{NN}}$ = 2.76 TeV. The region in the upper right corner encompassed by the dashed lines depicts the 0–0.2% selected centrality range.

Centrality selections of ultra-central events are investigated in Monte Carlo (MC) simulations using the AMPT [30] heavy-ion event generator, which provides a realistic modeling of the initial-state fluctuations of participating nucleons. The generated particles are propagated through the full GEANT4 [31] simulation of the CMS detector. The equivalent centrality requirements on the HF energy sum and pixel cluster multiplicity are applied in order to evaluate the selected ranges of impact parameter and number of participating nucleons, N_{Part}, for various centrality ranges. A summary of the mean and RMS values of N_{Part} distributions for selected events of each very central PbPb centrality range can be found in Table 1. As one can see, there is only a moderate increase of average N_{Part} value for events that are more central than 0–1% centrality, although the RMS value still decreases significantly for more central selections.

Table 1: The mean and RMS of N_{Part} distributions for selected events in each centrality bin in AMPT simulations.

Centrality	$\langle N_{Part} \rangle$	RMS
0–0.02%	406.2	3.6
0–0.2%	404.0	6.9
0–1.0%	401.1	8.3
0–2.5%	395.8	11.3
2.5–5.0%	381.3	19.5

Events are further selected offline by requiring energy deposits in at least three towers in each of the HF calorimeters, with at least 3 GeV of energy in each tower, and the presence of a reconstructed primary vertex containing at least two tracks. The reconstructed primary vertex is required to be located within $\pm$15 cm of the average interaction region along the beam axis and within a radius of 0.02 cm in the transverse plane. These criteria further reduce the background from single-beam interactions (e.g., beam-gas and beam-halo), cosmic muons, and ultra peripheral collisions that lead to the electromagnetic breakup of one or both Pb nuclei [32].

During the 2011 PbPb run, there was a probability of about 10^{-3} to have two collisions recorded in a single beam crossing (pileup events). This probability is even higher for ultra-central triggered events, which sample the tails of the HF energy sum and pixel cluster multiplicity distributions. If a large HF energy sum or pixel cluster multiplicity event is due to two mid-central collisions instead of a single ultra-central collision, more spectator neutrons will be released, resulting in a large signal in the ZDC. To select cleaner single-collision PbPb events, the correlation of energy sum signals between ZDC and HF detectors is studied. Events with large signals in both ZDC and HF are identified as pileup events (about 0.1% of all events), and thus rejected.

The reconstruction of the primary event vertex and the trajectories of charged particles in PbPb collisions is based on signals in the silicon pixel and strip detectors and described in detail in Ref. [8]. From studies based on PbPb events simulated using HYDJET [33] (version 1.8), the combined geometrical acceptance and reconstruction efficiency of the primary tracks is about 70% at $p_T \sim 1\,\text{GeV}/c$ and $|\eta| < 1.0$ for the 0–0.2% central PbPb events but drops to about 50% for $p_T \sim 0.3\,\text{GeV}/c$. The fraction of misidentified tracks is kept at the level of $< 5\%$ over most of the p_T ($p_T > 0.5\,\text{GeV}/c$) and η ($|\eta| < 1.6$) ranges. It increases up to about 20% for very low p_T ($p_T < 0.5\,\text{GeV}/c$) particles in the forward ($|\eta| \approx 2$) region.

4 Analysis procedure

Following the same procedure of dihadron correlation analysis as in Refs. [9, 34–37], the signal and background distributions of particle pairs are first constructed. Any charged particle associated with the primary vertex and in the range $|\eta| < 2.4$ can be used as a "trigger" particle. A variety of bins of trigger particle transverse momentum, denoted by $p_{\mathrm{T}}^{\mathrm{trig}}$, are considered. In a single event, there can be more than one trigger particle and their total multiplicity is denoted by N_{trig}. Within each event, every trigger particle is then paired with all of the remaining particles (again within $|\eta| < 2.4$). Just as for the trigger particles, these associated particles are also binned in transverse momentum ($p_{\mathrm{T}}^{\mathrm{assoc}}$).

The signal distribution, $S(\Delta\eta, \Delta\phi)$, is the per-trigger-particle yield of pairs found in the same event,

$$S(\Delta\eta, \Delta\phi) = \frac{1}{N_{\mathrm{trig}}} \frac{\mathrm{d}^2 N^{\mathrm{same}}}{\mathrm{d}\Delta\eta\, \mathrm{d}\Delta\phi}, \tag{1}$$

where N^{same} is the number of such pairs within a ($\Delta\eta$,$\Delta\phi$) bin, and $\Delta\phi$ and $\Delta\eta$ are the differences in azimuthal angle ϕ and pseudorapidity η between the two particles. The background distribution, $B(\Delta\eta, \Delta\phi)$, is found using a mixed-event technique, wherein trigger particles from one event are combined (mixed) with all of the associated particles from a different event. In the analysis, associated particles from 10 randomly chosen events with a small z_{vtx} range (± 0.5 cm) near the z_{vtx} of the event with trigger particles are used. The result is given by

$$B(\Delta\eta, \Delta\phi) = \frac{1}{N_{\mathrm{trig}}} \frac{\mathrm{d}^2 N^{\mathrm{mix}}}{\mathrm{d}\Delta\eta\, \mathrm{d}\Delta\phi}, \tag{2}$$

where N^{mix} denotes the number of mixed-event pairs. This background distribution represents the expected correlation function assuming independent particle emission, but taking into account effects of the finite acceptance.

The two-dimensional (2-D) differential yield of associated particles per trigger particle is given by

$$\frac{1}{N_{\mathrm{trig}}} \frac{\mathrm{d}^2 N^{\mathrm{pair}}}{\mathrm{d}\Delta\eta\, \mathrm{d}\Delta\phi} = B(0,0) \times \frac{S(\Delta\eta, \Delta\phi)}{B(\Delta\eta, \Delta\phi)}, \tag{3}$$

where N^{pair} is the total number of hadron pairs. The value of the background distribution at $\Delta\eta = 0$ and $\Delta\phi = 0$, $B(0,0)$, represents the mixed-event associated yield for both particles of the pair going in approximately the same direction and thus having full pair acceptance (with a bin width of 0.3 in $\Delta\eta$ and $\pi/16$ in $\Delta\phi$). Therefore, the ratio $B(0,0)/B(\Delta\eta, \Delta\phi)$ accounts for the pair-acceptance effects. The correlation function described in Eq. (3) is calculated in 0.5 cm wide bins of the z_{vtx} along the beam direction and then averaged over the range $|z_{\mathrm{vtx}}| < 15$ cm.

To extract the azimuthal anisotropy harmonics, v_n, the one-dimensional (1D) azimuthal dihadron correlation function as a function of $\Delta\phi$, averaged over $|\Delta\eta| > 2$ (to avoid the short-range correlations from jets and resonance decays), can be decomposed into a Fourier series given by

$$\frac{1}{N_{\mathrm{trig}}} \frac{\mathrm{d}N^{\mathrm{pair}}}{\mathrm{d}\Delta\phi} = \frac{N_{\mathrm{assoc}}}{2\pi} \left\{ 1 + \sum_{n=1}^{\infty} 2V_{n\Delta} \cos(n\Delta\phi) \right\}. \tag{4}$$

Here, $V_{n\Delta}$ are the Fourier coefficients from dihadron correlations, and N_{assoc} represents the total number of hadron pairs per trigger particle for a given $|\Delta\eta|$ range and ($p_{\mathrm{T}}^{\mathrm{trig}}$, $p_{\mathrm{T}}^{\mathrm{assoc}}$) bin.

In Refs. [9, 35–37], a fit to the azimuthal correlation function by a Fourier series was used to extract the $V_{n\Delta}$ coefficients. In this paper, a slightly different approach is applied. The $V_{n\Delta}$ values are directly calculated as the average value of $\cos(n\Delta\phi)$ of all particle pairs for $|\Delta\eta| > 2$ (to avoid the short-range correlations from jets and resonance decays):

$$V_{n\Delta} = \langle\langle\cos(n\Delta\phi)\rangle\rangle_S - \langle\langle\cos(n\Delta\phi)\rangle\rangle_B. \tag{5}$$

Here, $\langle\langle\ \rangle\rangle$ denotes averaging over all particles in each event and over all the events. The subscripts S and B correspond to the average over signal and background pairs. With an ideal detector, $\langle\langle\cos(n\Delta\phi)\rangle\rangle_S$ equals to $V_{n\Delta}$ by definition. The $\langle\langle\cos(n\Delta\phi)\rangle\rangle_B$ term is subtracted in order to remove the effects of detector non-uniformity. This is in principle equivalent to the fitting method based on Eq. (4). The advantage of the present approach is that the extracted Fourier harmonics will not be affected by the finite bin widths of the histogram in $\Delta\eta$ and $\Delta\phi$. This is particularly important for very-high-order harmonics ($V_{n\Delta}$ is extracted up to $n = 7$ in this analysis) that are sensitive to the finer variations of the correlation functions.

It was thought [9, 14, 16] that, for correlations purely driven by the hydrodynamic flow, $V_{n\Delta}$ can be factorized into a product of single-particle Fourier harmonics, $v_n(p_{\mathrm{T}}^{\mathrm{trig}})$, for trigger particles and $v_n(p_{\mathrm{T}}^{\mathrm{assoc}})$, for associated particles:

$$V_{n\Delta} = v_n(p_{\mathrm{T}}^{\mathrm{trig}}) \times v_n(p_{\mathrm{T}}^{\mathrm{assoc}}). \tag{6}$$

The single-particle azimuthal anisotropy harmonics can then be extracted as a function of p_{T} as follows:

$$v_n(p_{\mathrm{T}}) = \frac{V_{n\Delta}(p_{\mathrm{T}}, p_{\mathrm{T}}^{\mathrm{ref}})}{\sqrt{V_{n\Delta}(p_{\mathrm{T}}^{\mathrm{ref}}, p_{\mathrm{T}}^{\mathrm{ref}})}}, \tag{7}$$

where a fixed $p_{\mathrm{T}}^{\mathrm{ref}}$ range is chosen for the "reference particles". However, as pointed out in Refs. [26, 27], due to fluctuating initial-state geometry, the factorization of $V_{n\Delta}$ could also break down for flow-only correlations. Direct tests of the factorization relation for $V_{n\Delta}$ in Eq. (6) are carried out in this paper, as will be discussed in Section 5.3. These tests may provide new insights into the initial-state density fluctuations of the expanding hot medium.

When calculating $\langle\langle\cos(n\Delta\phi)\rangle\rangle$, each pair is weighted by the product of correction factors for the two particles. These factors are the inverse of an efficiency that is a function of each particle's pseudorapidity and transverse momentum,

$$\varepsilon_{\mathrm{trk}}(\eta, p_{\mathrm{T}}) = \frac{A(\eta, p_{\mathrm{T}})E(\eta, p_{\mathrm{T}})}{1 - F(\eta, p_{\mathrm{T}})}, \tag{8}$$

where $A(\eta, p_{\mathrm{T}})$ is the geometrical acceptance, $E(\eta, p_{\mathrm{T}})$ is the reconstruction efficiency, and $F(\eta, p_{\mathrm{T}})$ is the fraction of misidentified tracks. The effect of this weighting factor only changes the overall scale of dihadron correlation functions, and has almost no effect on $\langle\langle\cos(n\Delta\phi)\rangle\rangle$. However, the misidentified tracks may have different v_n values from those of correctly reconstructed tracks. Therefore, the effects of misidentified tracks are investigated and corrected using the same procedure as done in Ref. [8]. The v_n values for the true charged tracks (v_n^{true}) can be expressed as a combination of v_n for all the observed tracks (v_n^{obs}) and for misidentified tracks (v_n^{mis}):

$$v_n^{\mathrm{true}}(p_{\mathrm{T}}) = \frac{v_n^{\mathrm{obs}}(p_{\mathrm{T}}) - F(p_{\mathrm{T}}) \times v_n^{\mathrm{mis}}(p_{\mathrm{T}})}{1 - F(p_{\mathrm{T}})}. \tag{9}$$

An empirical correction for the misidentified track v_n based on the simulation studies is found to be independent of track selections or the fraction of misidentified tracks. The correction is

given by $v_n^{\mathrm{mis}} = f \times \langle v_n \rangle$, where $\langle v_n \rangle$ is the yield-weighted average over the p_{T} range from 0.3 to 3.0 GeV/c, folding in the efficiency-corrected spectra. The estimated values of the correction factor, f, as well as its uncertainty, are summarized in Table 2 for different v_n.

Table 2: The factor, f, for estimating the v_n values of misidentified tracks, as well as its uncertainty, for various orders of Fourier harmonics.

n	f
2	1.3 ± 0.1
3	1.0 ± 0.4
4	0.8 ± 0.6
5	0.8 ± 0.6
>6	0.8 ± 0.6

The systematic uncertainties due to misidentified tracks, which are most important at low p_{T} where the misidentified track rate is high, are reflected in the uncertainty of the f factor in Table 2. At low p_{T}, the systematic uncertainty from this source is 1.4% for v_2 and 5–8% for v_3 to v_6. By varying the z-coordinate of vertex binning in the mixed-event background, the results of the v_n values vary by at most 2–8% for v_2 to v_6, respectively. Systematic uncertainties due to the tracking efficiency correction are estimated to be about 0.5%. By varying the requirements on the ZDC sum energy used for pileup rejection, the results are stable within less than 1%. The various sources of systematic uncertainties are added in quadrature to obtain the final uncertainties shown as the shaded color bands for results in Section 5.

5 Results

5.1 Single-particle azimuthal anisotropy, v_n

Results of azimuthal anisotropy harmonics, from v_2 to v_6, as a function of p_{T} in 0–0.2% central PbPb collisions at $\sqrt{s_{NN}}$ = 2.76 TeV, are shown in Fig. 2 (left). The v_n values are extracted from long-range ($|\Delta\eta| > 2$) dihadron correlations using Eq. (5), and by assuming factorization in Eq. (7). The $p_{\mathrm{T}}^{\mathrm{ref}}$ range is chosen to be 1–3 GeV/c. The error bars correspond to statistical uncertainties, while the shaded color bands indicate the systematic uncertainties. As the collisions are extremely central, the eccentricities, ϵ_{n}, are mostly driven by event-by-event participant fluctuations and are of similar sizes within a few % for all orders. Consequently, the magnitudes of v_2 and v_3 are observed to be comparable (within 2% averaged over p_{T} as will be shown in Fig. 4), which is not the case for non-central collisions. Different v_n harmonics have very different dependencies on p_{T}. At low p_{T} ($p_{\mathrm{T}} < 1$ GeV/c), the v_2 harmonic has the biggest magnitude compared to other higher-order harmonics. It becomes smaller than v_3 at $p_{\mathrm{T}} \approx 1$ GeV/c, and even smaller than v_5 for $p_{\mathrm{T}} > 3$ GeV/c. This intriguing p_{T} dependence can be compared quantitatively to hydrodynamics calculations with fluctuating initial conditions, and it provides important constraints on theoretical models. For a given value of p_{T}, the magnitude of v_n for $n \geq 3$ decreases monotonically with n, as will be shown later.

If a system created in an ultra-relativistic heavy-ion collision behaves according to ideal hydrodynamics, the Fourier harmonics, v_n, are expected to follow a p_{T} dependence that has a power-law, p_{T}^n, functional form in the low-p_{T} region [38, 39]. Hence, the scaling ratio, $v_n^{1/n}/v_2^{1/2}$, will be largely independent of p_{T}, as was seen by the ATLAS collaboration for not very central events [16]. In Fig. 2 (right), the $v_n^{1/n}/v_2^{1/2}$ ratios are shown as a function of p_{T} for n = 3–6

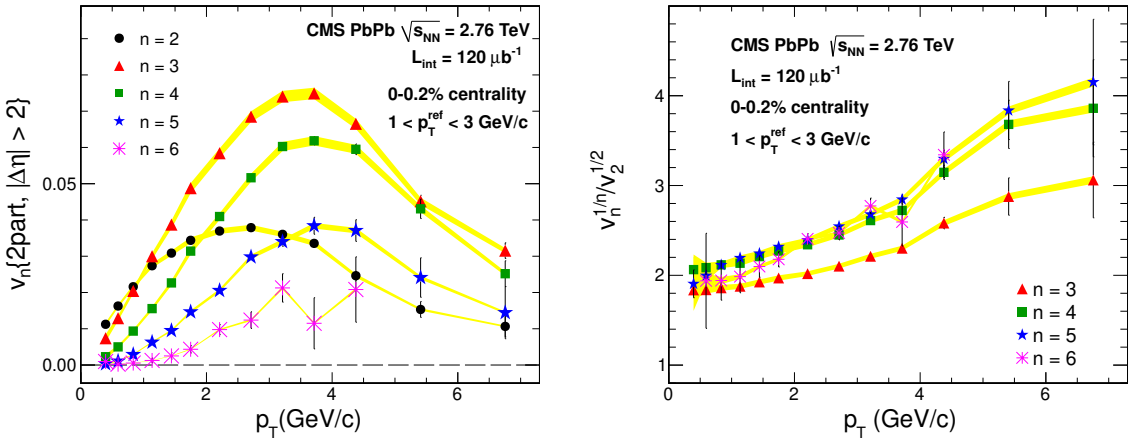

Figure 2: Left: the v_2 to v_6 values as a function of p_T in 0–0.2% central PbPb collisions at $\sqrt{s_{NN}}$ = 2.76 TeV. Right: the $v_n^{1/n}/v_2^{1/2}$ ratios as a function of p_T. Error bars denote the statistical uncertainties, while the shaded color bands correspond to the systematic uncertainties.

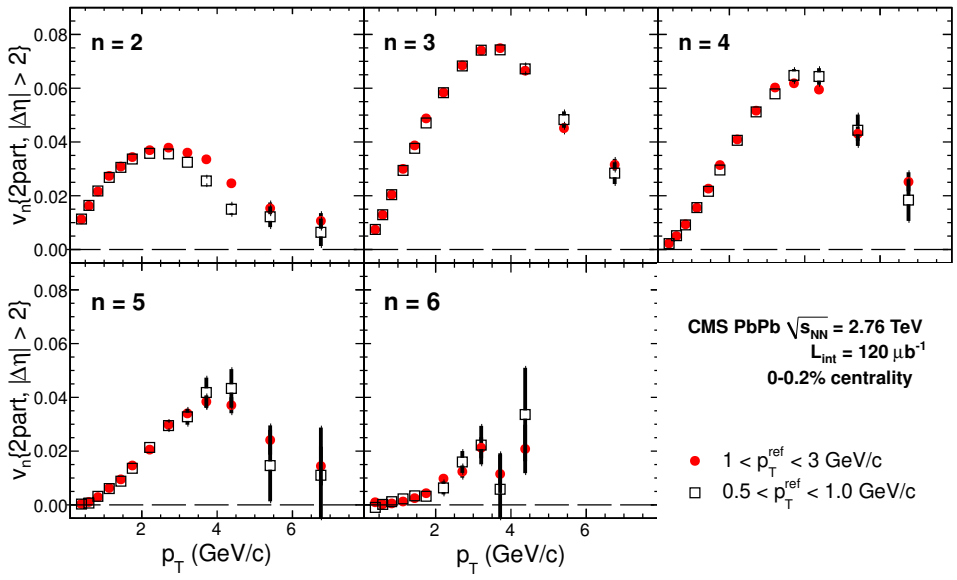

Figure 3: Comparison of $v_n(p_T)$ values derived from two different p_T^{ref} ranges: 0.5–1.0 GeV/c (open square markers) and 1–3 GeV/c (solid circles), in 0–0.2% central PbPb collisions at $\sqrt{s_{NN}}$ = 2.76 TeV. Error bars denote the statistical uncertainties.

obtained in 0–0.2% ultra-central PbPb collisions at $\sqrt{s_{NN}}$ = 2.76 TeV. The obtained ratio shows an increase as a function of p_T. This trend is consistent to what was observed by the ATLAS collaboration for very central events (e.g., 0–1% centrality) [16].

Other choices of p_T^{ref} ranges are also studied in order to examine the assumption of factorization made for extracting v_n. As an example, Fig. 3 shows the comparison of v_n as a function of p_T for $1 < p_T^{ref} < 3$ GeV/c and $0.5 < p_T^{ref} < 1.0$ GeV/c. The v_n values extracted with two choices of p_T^{ref} ranges are consistent within statistical uncertainties for $n > 2$ over the entire p_T range. However, a large discrepancy is observed for v_2 at higher p_T, e.g., up to about 40% for $p_T \sim 4$ GeV/c, while the low p_T region shows a good agreement between the two p_T^{ref} ranges. A detailed study of factorization breakdown for Eq. (6) as well as its physical implication is

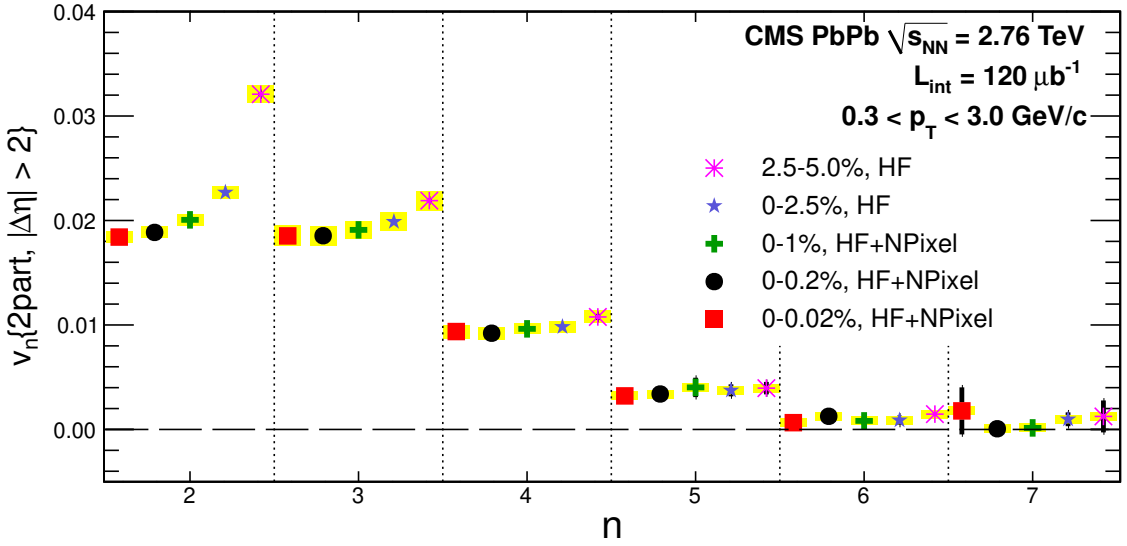

Figure 4: Comparison of p_T-averaged (0.3–3.0 GeV/c) v_n as a function of n in five centrality ranges (2.5–5.0%, 0–2.5%, 0–1%, 0–0.2% and 0–0.02%) for PbPb collisions at $\sqrt{s_{NN}}$ = 2.76 TeV. The p_T^{ref} of 1–3 GeV/c is used. Error bars denote the statistical uncertainties, while the shaded color boxes correspond to the systematic uncertainties.

presented in Section 5.3.

The p_T-averaged v_n values (with p_T^{ref} of 1–3 GeV/c) weighted by the efficiency-corrected charged-hadron yield, over the p_T range from 0.3 to 3.0 GeV/c, are shown in Fig. 4 as a function of n up to $n = 7$ (the v_7 value as a function of p_T is not presented in Fig. 2 due to limited statistical precision). The 0–0.2% ultra-central events are compared to several other very central PbPb centrality ranges including 2.5–5.0%, 0–2.5%, 0–1% and 0–0.02%. As mentioned earlier, results for 0–1% centrality are compared with both the HF energy sum selection (not shown) and HF energy sum plus pixel cluster multiplicity (NPixel) selection as a systematic check. The two methods of centrality selection yield consistent v_n results within statistical uncertainties. Therefore, only results from HF energy sum plus pixel cluster multiplicity centrality selection are shown in Fig. 4. Beyond the 2.5–5.0% centrality range, the v_n values are still decreasing toward more central collisions, especially for v_2. Going from 0–0.2% to 0–0.02% centrality, v_n shows almost no change, indicating events do not become significantly more central by requiring larger HF energy sum and pixel cluster multiplicity, especially in terms of eccentricities. This is consistent with the studies using the AMPT model. The v_n values remain finite up to $n = 6$ within the statistical precision of our data. Beyond $n = 6$, v_n becomes consistent with zero. The magnitude of v_2 and v_3 are very similar, while the v_n become progressively smaller for $n \geq 4$. This is qualitatively in agreement with expectations from hydrodynamic calculations [38].

5.2 Correlation Functions

Dihadron correlation functions are also constructed using Eq. (3) in order to check the consistency of extracting $V_{n\Delta}$ using Eq. (5) with the fit method to the correlation function by a Fourier series in Eq. (4). Figure 5 (left) shows the dihadron correlation functions for $1 < p_T^{trig} < 3$ GeV/c and $1 < p_T^{assoc} < 3$ GeV/c in 0–0.2% central PbPb collisions at $\sqrt{s_{NN}}$ = 2.76 TeV. As shown in Fig. 2, the v_3, v_4, and v_5 values become comparable or even bigger than v_2 at $1 < p_T < 3$ GeV/c.

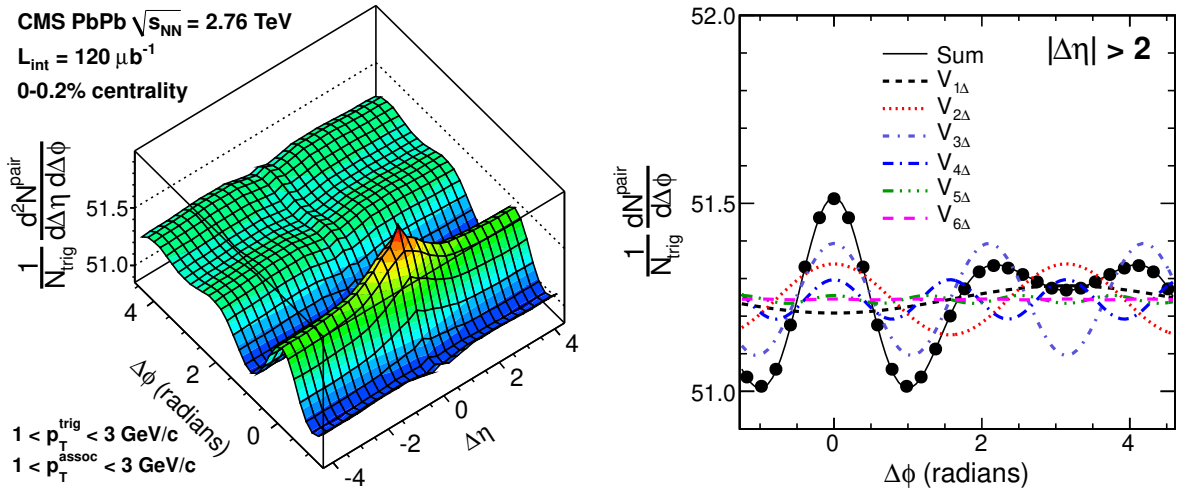

Figure 5: The 2D (left) and 1D $\Delta\phi$ (right) dihadron correlation functions for $1 < p_T^{trig} < 3\,\text{GeV}/c$ and $1 < p_T^{assoc} < 3\,\text{GeV}/c$ in 0–0.2% central PbPb collisions at $\sqrt{s_{NN}} = 2.76\,\text{TeV}$. The solid lines on the right panel show various orders of $V_{n\Delta}$ components expected from the extracted v_n values in Section 5.1, while the dashed line is the sum of all $V_{n\Delta}$ components.

In Fig. 5, this can be seen in the dihadron correlation function on the away side ($\Delta\phi \sim \pi$), where a significant local minimum (at $\Delta\phi \sim \pi$ along $\Delta\eta$) is present. On the near side ($\Delta\phi \sim 0$) of the correlation function, a long-range structure extending over the entire $\Delta\eta$ region is present. The observed features of the correlation function are similar to what was seen previously at CMS in other centrality ranges of PbPb collisions [9, 35], although the dip on the away side is not seen in non-central PbPb collisions. This may indicate that the contribution of higher-order Fourier components (e.g., v_3) is more relevant for very central events.

Averaging over $\Delta\eta$, the 1D $\Delta\phi$ dihadron correlation function, for $1 < p_T^{trig} < 3\,\text{GeV}/c$ and $1 < p_T^{assoc} < 3\,\text{GeV}/c$ in 0–0.2% central PbPb collisions at $\sqrt{s_{NN}} = 2.76\,\text{TeV}$, is shown in Fig. 5 (right). The range of $|\Delta\eta| < 2$ is excluded from the average to avoid non-flow effects from other source of correlations, such as jet fragmentation. The dashed curves represent different $V_{n\Delta}$ components and are constructed from the v_n values extracted in Section 5.1 by assuming factorization. The solid curve is the sum of all $V_{n\Delta}$ components, which is in good agreement with the measured dihadron correlation function.

5.3 Factorization breakdown and p_T dependence of event plane angle

The breakdown of factorization observed in Fig. 3 could be caused by non-flow effects that contribute to the dihadron correlation function at large $\Delta\eta$, e.g., back-to-back jet correlations. However, in hydrodynamics, it has been recently suggested that one possible source of factorization breakdown is related to the initial-state eccentricity fluctuations [26, 27]. The event plane angle, Ψ_n, as determined by final-state particles, could be dependent on the particle p_T event-by-event, instead of a unique angle for the entire event (which is the case for a non-fluctuating smooth initial condition). Because of this effect, the factorization of $V_{n\Delta}$ extracted from dihadron correlations could be broken, even if hydrodynamic flow is the only source of correlations. The breakdown effect can be explored more quantitatively in the following analysis.

A ratio for testing factorization defined as

$$r_n \equiv \frac{V_{n\Delta}(p_{\mathrm{T}}^{\mathrm{trig}}, p_{\mathrm{T}}^{\mathrm{assoc}})}{\sqrt{V_{n\Delta}(p_{\mathrm{T}}^{\mathrm{trig}}, p_{\mathrm{T}}^{\mathrm{trig}}) V_{n\Delta}(p_{\mathrm{T}}^{\mathrm{assoc}}, p_{\mathrm{T}}^{\mathrm{assoc}})}} \tag{10}$$

has been proposed as a direct measurement of p_{T}-dependent event plane angle fluctuations [27]. Here, the $V_{n\Delta}$ coefficients are calculated by pairing particles within the same p_{T} interval (denominator) or from different p_{T} intervals (numerator). If $V_{n\Delta}$ factorizes, this ratio will be equal to unity. With the presence of a p_{T}-dependent event plane angle, it has been shown that the ratio, r_n, is equivalent to

$$r_n = \frac{\langle v_n(p_{\mathrm{T}}^{\mathrm{trig}}) v_n(p_{\mathrm{T}}^{\mathrm{assoc}}) \cos\left[n\left(\Psi_n(p_{\mathrm{T}}^{\mathrm{trig}}) - \Psi_n(p_{\mathrm{T}}^{\mathrm{assoc}})\right)\right]\rangle}{\sqrt{\langle v_n^2(p_{\mathrm{T}}^{\mathrm{trig}})\rangle \langle v_n^2(p_{\mathrm{T}}^{\mathrm{assoc}})\rangle}}, \tag{11}$$

where $\Psi_n(p_{\mathrm{T}}^{\mathrm{trig}})$ and $\Psi_n(p_{\mathrm{T}}^{\mathrm{assoc}})$ represent the event plane angles determined for trigger and associated particles from two p_{T} intervals [26, 27]. One can see from Eq. (11) that r_n is in general less than unity if event plane angle Ψ_n depends on p_{T}.

In this paper, the proposed factorization ratio, r_n, is studied as a function of $p_{\mathrm{T}}^{\mathrm{trig}}$ and $p_{\mathrm{T}}^{\mathrm{assoc}}$ for different centrality classes in PbPb collisions at $\sqrt{s_{NN}}$ = 2.76 TeV. Figures 6–8 show the r_n values for n = 2–4, respectively, for four $p_{\mathrm{T}}^{\mathrm{trig}}$ bins (of increasing p_{T} from left to right panels) as a function of the difference between $p_{\mathrm{T}}^{\mathrm{trig}}$ and $p_{\mathrm{T}}^{\mathrm{assoc}}$. The average values of $p_{\mathrm{T}}^{\mathrm{trig}}$ and $p_{\mathrm{T}}^{\mathrm{assoc}}$ in each bin are used for calculating the difference. The measurement is performed in four different centrality classes, i.e., 40–50%, 0–10%, 0–5%, and ultra-central 0–0.2% centralities (from bottom to top panels). By construction, the r_n value for the highest analyzed $p_{\mathrm{T}}^{\mathrm{assoc}}$ range, where trigger and associated particles are selected from the same p_{T} interval, is equal to one. Only results for $p_{\mathrm{T}}^{\mathrm{trig}} \geq p_{\mathrm{T}}^{\mathrm{assoc}}$ are presented. The error bars correspond to statistical uncertainties, while systematic uncertainties are negligible for the r_n ratios, and thus are not presented in the figures.

For the second Fourier harmonics (Fig. 6), the r_2 ratio significantly deviates from one as the collisions become more central. For any centrality, the effect gets larger with an increase of the difference between $p_{\mathrm{T}}^{\mathrm{trig}}$ and $p_{\mathrm{T}}^{\mathrm{assoc}}$ values. The deviation reaches up to 20% for the lowest $p_{\mathrm{T}}^{\mathrm{assoc}}$ bins in the ultra-central 0–0.2% events for $2.5 < p_{\mathrm{T}}^{\mathrm{trig}} < 3.0$. This is expected as event-by-event initial-state geometry fluctuations play a more dominant role as the collisions become more central. Calculations from viscous hydrodynamics in Ref. [27] are compared to data for 0–10% and 40–50% centralities with MC Glauber initial condition model [40, 41] and $\eta/s = 0.08$ (dashed lines), and MC-KLN initial condition model [42] and $\eta/s = 0.2$ (solid lines). The qualitative trend of hydrodynamic calculations is the same as what is observed in the data. The observed r_2 values are found to be more consistent with the MC-KLN model and an η/s value of 0.2. However, future theoretical studies, particularly with comparison to the precision ultra-central collisions data presented in this paper, are still needed to achieve better constraints on the initial-state models and the η/s value of the system.

For higher-order harmonics ($n = 3, 4$), shown in Fig. 7 and Fig. 8, the factorization is fulfilled over a wider range of $p_{\mathrm{T}}^{\mathrm{trig}}$, $p_{\mathrm{T}}^{\mathrm{assoc}}$, and centrality ranges than for v_2. The factorization only breaks by about 5% at large values of $p_{\mathrm{T}}^{\mathrm{trig}} - p_{\mathrm{T}}^{\mathrm{assoc}}$, i.e., greater than 1 GeV/c. Due to large statistical uncertainties, r_5 is not included in this result. Again, the qualitative trend of the data is described by hydrodynamics for 0–10% centrality, while no conclusion can be drawn for 40–50% centrality based on the present statistical precision of the data.

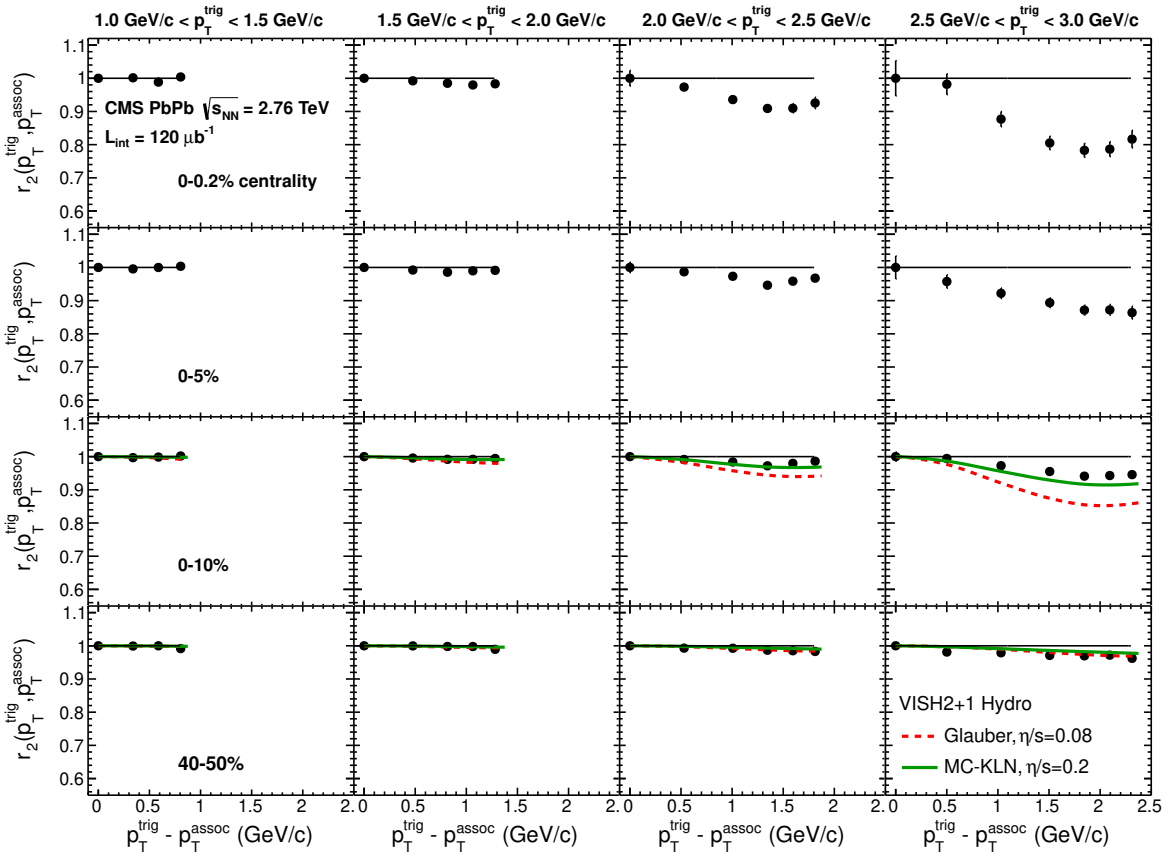

Figure 6: Factorization ratio, r_2, as a function of $p_{\mathrm{T}}^{\mathrm{trig}}$ - $p_{\mathrm{T}}^{\mathrm{assoc}}$ in bins of $p_{\mathrm{T}}^{\mathrm{trig}}$ for four centrality ranges of PbPb collisions at $\sqrt{s_{NN}}$ = 2.76 TeV. The lines show the calculations from viscous hydrodynamics in Ref. [27] for 0–10% and 40–50% centralities with MC Glauber initial condition model and $\eta/s = 0.08$ (dashed lines), and MC-KLN initial condition model and $\eta/s = 0.2$ (solid lines). Each row represents different centrality range, while each column corresponds to different $p_{\mathrm{T}}^{\mathrm{trig}}$ range. The error bars correspond to statistical uncertainties, while systematic uncertainties are negligible for the r_n ratios, and thus are not presented.

6 Conclusion

In summary, azimuthal dihadron correlations were studied for PbPb collisions at $\sqrt{s_{NN}} = 2.76$ TeV using the CMS detector at the LHC. Assuming factorization, these two-particle correlations were used to extract the single-particle anisotropy harmonics, v_n, as a function of p_{T} from 0.3 to 8.0 GeV/c. The data set includes a sample of ultra-central (0–0.2% centrality) PbPb events collected using a trigger based on total transverse energy in the hadron forward calorimeters and the total multiplicity of pixel clusters in the silicon pixel tracker. In the context of hydrodynamic models, anisotropies in such ultra-central heavy-ion collisions arise predominantly from initial-state eccentricity fluctuations. The magnitude of the flow harmonics decreases from v_3 to v_6. As a function of p_{T}, these four harmonics all display a common maximum around $p_{\mathrm{T}} = 3.5$ GeV/c. Although the v_2 harmonic exceeds the others at low p_{T}, it falls below v_3 around $p_{\mathrm{T}} = 1$ GeV/c and reaches its maximum around $p_{\mathrm{T}} = 2.5$ GeV/c.

The p_{T}-averaged v_n for $0.3 < p_{\mathrm{T}} < 3.0$ GeV/c were also derived up to $n = 7$, and results for 0–0.2% collisions were compared to those for other slightly less central ranges. Between the 2.5–5.0% and 0–0.2% centrality ranges, all v_n harmonics decrease. The decrease is largest for

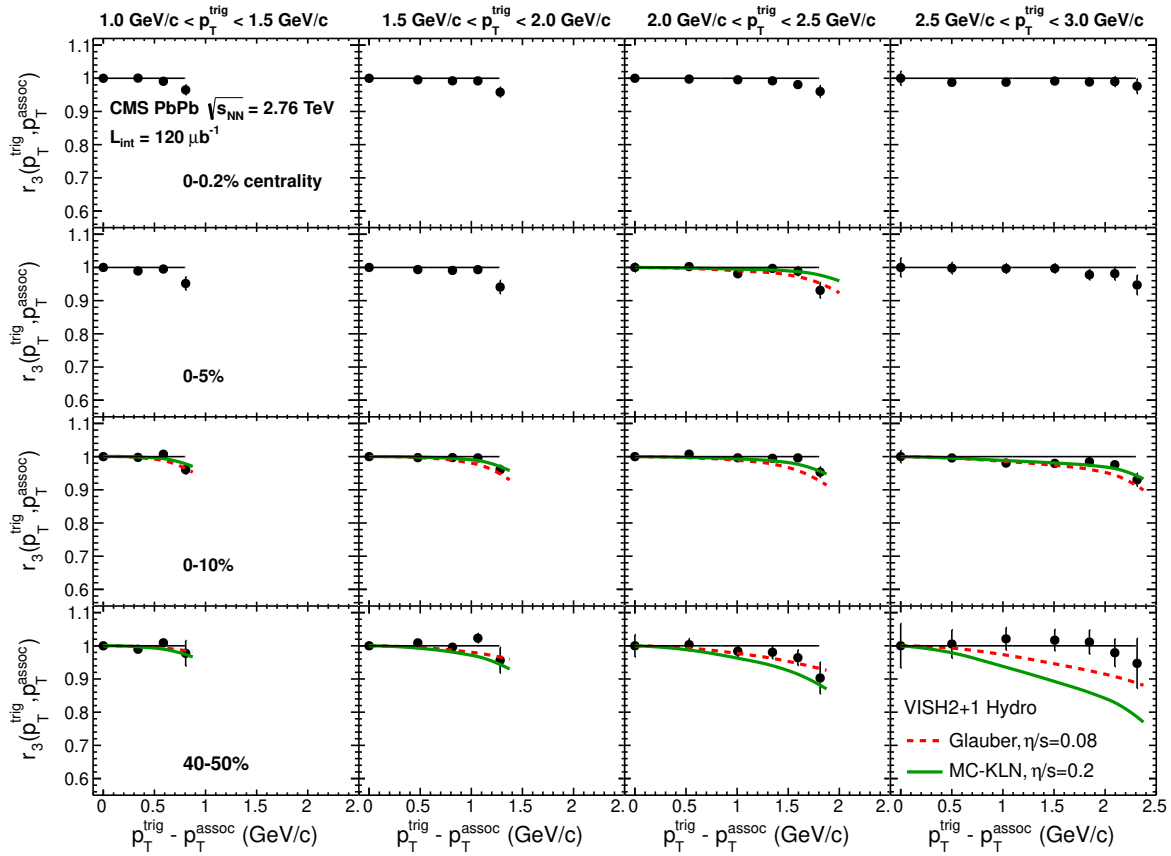

Figure 7: Factorization ratio, r_3, as a function of $p_{\mathrm{T}}^{\mathrm{trig}}$ - $p_{\mathrm{T}}^{\mathrm{assoc}}$ in bins of $p_{\mathrm{T}}^{\mathrm{trig}}$ for four centrality ranges of PbPb collisions at $\sqrt{s_{NN}}$ = 2.76 TeV. The lines show the calculations from viscous hydrodynamics in Ref. [27] for 0–10% and 40–50% centralities with MC Glauber initial condition model and $\eta/s = 0.08$ (dashed lines), and MC-KLN initial condition model and $\eta/s = 0.2$ (solid lines). Each row represents different centrality range, while each column corresponds to different $p_{\mathrm{T}}^{\mathrm{trig}}$ range. The error bars correspond to statistical uncertainties, while systematic uncertainties are negligible for the r_n ratios, and thus are not presented.

v_2, reaching up to 45%. Only small variations of v_n are observed for events that are even more central than 0–0.2% (e.g., 0–0.02%). For the most central collisions, the p_{T}-averaged v_2 and v_3 are found to be comparable within 2%, while higher-order v_n decrease as n increases.

Detailed studies indicate that factorization of dihadron correlations into single-particle azimuthal anisotropies does not hold precisely. The observed breakdown of factorization increases up to about 20% as the p_{T} difference between the two particles becomes larger in ultra-central PbPb events. This behavior is expected in hydrodynamic models, in which a p_{T}-dependent event plane angle is induced by initial-state fluctuations. The factorization data for the 0–10% and 40–50% centrality ranges were compared to viscous hydrodynamic calculations with different models of initial-state fluctuations and different η/s values. Future quantitative theoretical comparisons to the high-precision data of ultra-central PbPb collisions presented by the CMS collaboration in this paper can provide a new stringent test of hydrodynamic models, particularly for constraining the initial-state density fluctuations and the η/s value.

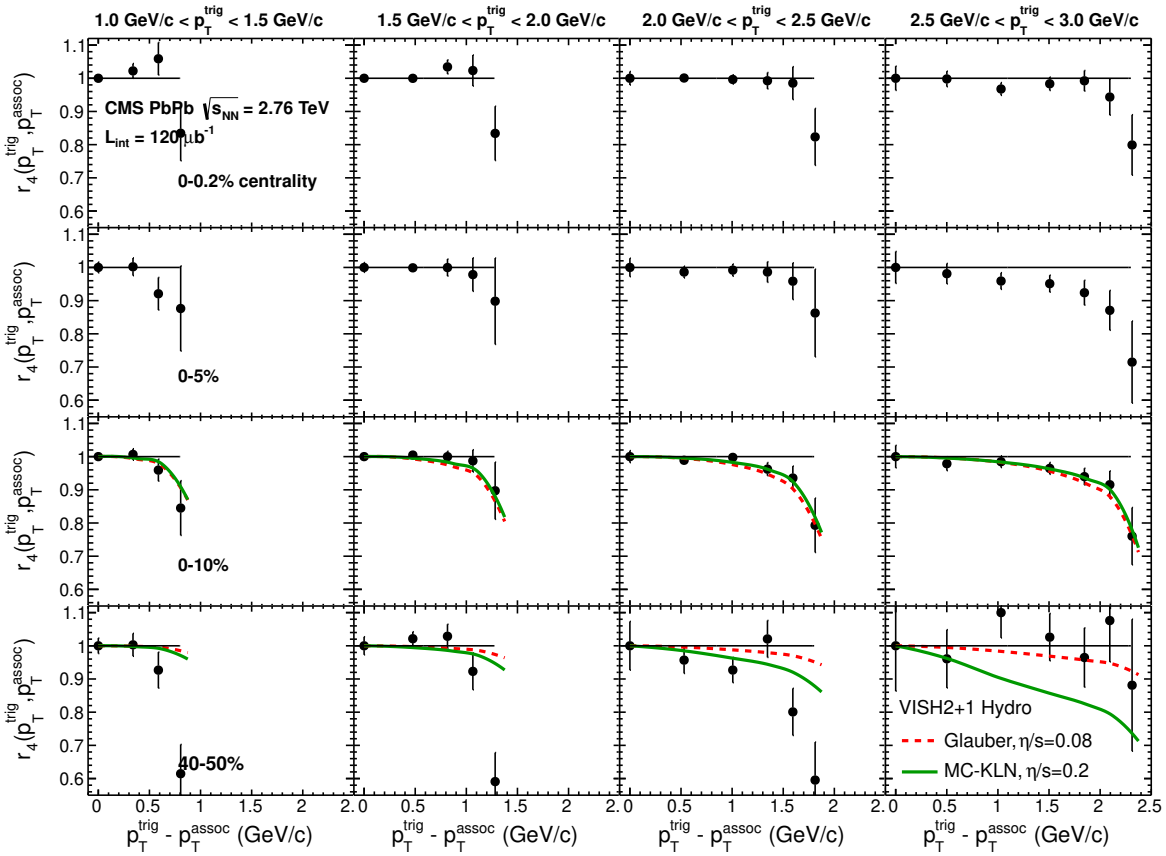

Figure 8: Factorization ratio, r_4, as a function of $p_{\mathrm{T}}^{\mathrm{trig}}$ - $p_{\mathrm{T}}^{\mathrm{assoc}}$ in bins of $p_{\mathrm{T}}^{\mathrm{trig}}$ for four centrality ranges of PbPb collisions at $\sqrt{s_{NN}}$ = 2.76 TeV. The lines show the calculations from viscous hydrodynamics in Ref. [27] for 0–10% and 40–50% centralities with MC Glauber initial condition model and $\eta/s = 0.08$ (dashed lines), and MC-KLN initial condition model and $\eta/s = 0.2$ (solid lines). Each row represents different centrality range, while each column corresponds to different $p_{\mathrm{T}}^{\mathrm{trig}}$ range. The error bars correspond to statistical uncertainties, while systematic uncertainties are negligible for the r_n ratios, and thus are not presented.

7 Acknowledgment

We congratulate our colleagues in the CERN accelerator departments for the excellent performance of the LHC and thank the technical and administrative staffs at CERN and at other CMS institutes for their contributions to the success of the CMS effort. In addition, we gratefully acknowledge the computing centres and personnel of the Worldwide LHC Computing Grid for delivering so effectively the computing infrastructure essential to our analyses. Finally, we acknowledge the enduring support for the construction and operation of the LHC and the CMS detector provided by the following funding agencies: BMWF and FWF (Austria); FNRS and FWO (Belgium); CNPq, CAPES, FAPERJ, and FAPESP (Brazil); MES (Bulgaria); CERN; CAS, MoST, and NSFC (China); COLCIENCIAS (Colombia); MSES (Croatia); RPF (Cyprus); MoER, SF0690030s09 and ERDF (Estonia); Academy of Finland, MEC, and HIP (Finland); CEA and CNRS/IN2P3 (France); BMBF, DFG, and HGF (Germany); GSRT (Greece); OTKA and NKTH (Hungary); DAE and DST (India); IPM (Iran); SFI (Ireland); INFN (Italy); NRF and WCU (Republic of Korea); LAS (Lithuania); CINVESTAV, CONACYT, SEP, and UASLP-FAI (Mexico); MBIE (New Zealand); PAEC (Pakistan); MSHE and NSC (Poland); FCT (Portugal); JINR (Dubna); MON, RosAtom, RAS and RFBR (Russia); MESTD (Serbia); SEIDI and CPAN (Spain);

Swiss Funding Agencies (Switzerland); NSC (Taipei); ThEPCenter, IPST, STAR and NSTDA (Thailand); TUBITAK and TAEK (Turkey); NASU (Ukraine); STFC (United Kingdom); DOE and NSF (USA).

Individuals have received support from the Marie-Curie programme and the European Research Council and EPLANET (European Union); the Leventis Foundation; the A. P. Sloan Foundation; the Alexander von Humboldt Foundation; the Belgian Federal Science Policy Office; the Fonds pour la Formation à la Recherche dans l'Industrie et dans l'Agriculture (FRIA-Belgium); the Agentschap voor Innovatie door Wetenschap en Technologie (IWT-Belgium); the Ministry of Education, Youth and Sports (MEYS) of Czech Republic; the Council of Science and Industrial Research, India; the Compagnia di San Paolo (Torino); the HOMING PLUS programme of Foundation for Polish Science, cofinanced by EU, Regional Development Fund; and the Thalis and Aristeia programmes cofinanced by EU-ESF and the Greek NSRF.

References

[1] U. Heinz and R. Snellings, "Collective flow and viscosity in relativistic heavy-ion collisions", *Ann. Rev. Nucl. Part. Sci.* **63** (2013) 123, doi:10.1146/annurev-nucl-102212-170540, arXiv:1301.2826.

[2] PHENIX Collaboration, "Formation of dense partonic matter in relativistic nucleus-nucleus collisions at RHIC: Experimental evaluation by the PHENIX collaboration", *Nucl. Phys. A* **757** (2005) 184, doi:10.1016/j.nuclphysa.2005.03.086, arXiv:nucl-ex/0410003.

[3] STAR Collaboration, "Experimental and theoretical challenges in the search for the quark gluon plasma: The STAR Collaboration's critical assessment of the evidence from RHIC collisions", *Nucl. Phys. A* **757** (2005) 102, doi:10.1016/j.nuclphysa.2005.03.085, arXiv:nucl-ex/0501009.

[4] PHOBOS Collaboration, "The PHOBOS perspective on discoveries at RHIC", *Nucl. Phys. A* **757** (2005) 28, doi:10.1016/j.nuclphysa.2005.03.084, arXiv:nucl-ex/0410022.

[5] BRAHMS Collaboration, "Quark gluon plasma and color glass condensate at RHIC? The Perspective from the BRAHMS experiment", *Nucl. Phys. A* **757** (2005) 1, doi:10.1016/j.nuclphysa.2005.02.130, arXiv:nucl-ex/0410020.

[6] E. V. Shuryak, "What RHIC experiments and theory tell us about properties of quark-gluon plasma?", *Nucl. Phys. A* **750** (2005) 64, doi:10.1016/j.nuclphysa.2004.10.022, arXiv:hep-ph/0405066.

[7] M. Gyulassy and L. McLerran, "New forms of QCD matter discovered at RHIC", *Nucl. Phys. A* **750** (2005) 30, doi:10.1016/j.nuclphysa.2004.10.034, arXiv:nucl-th/0405013.

[8] CMS Collaboration, "Measurement of the elliptic anisotropy of charged particles produced in PbPb collisions at nucleon-nucleon center-of-mass energy = 2.76 TeV", *Phys. Rev. C* **87** (2013) 014902, doi:10.1103/PhysRevC.87.014902, arXiv:1204.1409.

[9] CMS Collaboration, "Centrality dependence of dihadron correlations and azimuthal anisotropy harmonics in PbPb collisions at $\sqrt{s_{NN}}$ = 2.76 TeV", *Eur. Phys. J. C* **72** (2012) 2012, doi:10.1140/epjc/s10052-012-2012-3, arXiv:1201.3158.

[10] CMS Collaboration, "Azimuthal anisotropy of charged particles at high transverse momenta in PbPb collisions at $\sqrt{s_{NN}}$ = 2.76 TeV", *Phys. Rev. Lett.* **109** (2012) 022301, doi:10.1103/PhysRevLett.109.022301, arXiv:1204.1850.

[11] CMS Collaboration, "Measurement of the azimuthal anisotropy of neutral pions in PbPb collisions at $\sqrt{s_{NN}}$ = 2.76 TeV", *Phys. Rev. Lett.* **110** (2013) 042301, doi:10.1103/PhysRevLett.110.042301, arXiv:1208.2470.

[12] ALICE Collaboration, "Elliptic flow of charged particles in Pb-Pb collisions at 2.76 TeV", *Phys. Rev. Lett.* **105** (2010) 252302, doi:10.1103/PhysRevLett.105.252302, arXiv:1011.3914.

[13] ALICE Collaboration, "Higher harmonic anisotropic flow measurements of charged particles in Pb-Pb collisions at $\sqrt{s_{NN}}$ = 2.76 TeV", *Phys. Rev. Lett.* **107** (2011) 032301, doi:10.1103/PhysRevLett.107.032301, arXiv:1105.3865.

[14] ALICE Collaboration, "Harmonic decomposition of two-particle angular correlations in Pb-Pb collisions at $\sqrt{s_{NN}}$ = 2.76 TeV", *Phys. Lett. B* **708** (2012) 249, doi:10.1016/j.physletb.2012.01.060, arXiv:1109.2501.

[15] ATLAS Collaboration, "Measurement of the pseudorapidity and transverse momentum dependence of the elliptic flow of charged particles in lead-lead collisions at $\sqrt{s_{NN}}$ = 2.76 TeV with the ATLAS detector", *Phys. Lett. B* **707** (2012) 330, doi:10.1016/j.physletb.2011.12.056, arXiv:1108.6018.

[16] ATLAS Collaboration, "Measurement of the azimuthal anisotropy for charged particle production in $\sqrt{s_{NN}}$ = 2.76 TeV lead-lead collisions with the ATLAS detector", *Phys. Rev. C* **86** (2012) 014907, doi:10.1103/PhysRevC.86.014907, arXiv:1203.3087.

[17] ATLAS Collaboration, "Measurement of the distributions of event-by-event flow harmonics in lead–lead collisions at $\sqrt{s_{NN}}$ = 2.76 TeV with the ATLAS detector at the LHC", (2013). arXiv:1305.2942.

[18] PHOBOS Collaboration, "Event-by-Event Fluctuations of Azimuthal Particle Anisotropy in Au + Au Collisions at $\sqrt{s_{NN}}$ = 200 GeV", *Phys. Rev. Lett.* **104** (2010) 142301, doi:10.1103/PhysRevLett.104.142301, arXiv:nucl-ex/0702036.

[19] B. Alver et al., "Importance of correlations and fluctuations on the initial source eccentricity in high-energy nucleus-nucleus collisions", *Phys. Rev. C* **77** (2008) 014906, doi:10.1103/PhysRevC.77.014906, arXiv:0711.3724.

[20] R. S. Bhalerao and J.-Y. Ollitrault, "Eccentricity fluctuations and elliptic flow at RHIC", *Phys. Lett. B* **641** (2006) 260, doi:10.1016/j.physletb.2006.08.055, arXiv:nucl-th/0607009.

[21] S. A. Voloshin, A. M. Poskanzer, A. Tang, and G. Wang, "Elliptic flow in the Gaussian model of eccentricity fluctuations", *Phys. Lett. B* **659** (2008) 537, doi:10.1016/j.physletb.2007.11.043, arXiv:0708.0800.

[22] J.-Y. Ollitrault, A. M. Poskanzer, and S. A. Voloshin, "Effect of flow fluctuations and nonflow on elliptic flow methods", *Phys. Rev. C* **80** (2009) 014904, doi:10.1103/PhysRevC.80.014904, arXiv:0904.2315.

[23] B. Alver and G. Roland, "Collision geometry fluctuations and triangular flow in heavy-ion collisions", *Phys. Rev. C* **81** (2010) 054905, doi:10.1103/PhysRevC.81.054905, arXiv:1003.0194.

[24] Z. Qiu and U. W. Heinz, "Event-by-event shape and flow fluctuations of relativistic heavy-ion collision fireballs", *Phys. Rev. C* **84** (2011) 024911, doi:10.1103/PhysRevC.84.024911, arXiv:1104.0650.

[25] M. Luzum and J.-Y. Ollitrault, "Extracting the shear viscosity of the quark-gluon plasma from flow in ultra-central heavy-ion collisions", *Nucl. Phys. A* **904** (2013) 377, doi:10.1016/j.nuclphysa.2013.02.028, arXiv:1210.6010.

[26] F. G. Gardim, F. Grassi, M. Luzum, and J.-Y. Ollitrault, "Breaking of factorization of two-particle correlations in hydrodynamics", *Phys. Rev. C* **87** (2012) 031901, doi:10.1103/PhysRevC.87.031901, arXiv:1211.0989.

[27] U. W. Heinz, Z. Qiu, and C. Shen, "Fluctuating flow angles and anisotropic flow measurements", *Phys. Rev. C* **87** (2013) 034913, doi:10.1103/PhysRevC.87.034913, arXiv:1302.3535.

[28] CMS Collaboration, "The CMS experiment at the CERN LHC", *JINST* **3** (2008) S08004, doi:10.1088/1748-0221/3/08/S08004.

[29] CMS Collaboration, O. A. Grachov et al., "Performance of the combined zero degree calorimeter for CMS", in *XXX Int. Conf. on Calorimetry in High Energy Physics (CALOR 2008)*, M. Livan, ed. 2009. arXiv:0807.0785. J. Phys.: Conf. Series, 160. doi:10.1088/1742-6596/160/1/012059.

[30] Z.-W. Lin et al., "A Multi-phase transport model for relativistic heavy ion collisions", *Phys. Rev. C* **72** (2005) 064901, doi:10.1103/PhysRevC.72.064901, arXiv:nucl-th/0411110.

[31] Geant4 Collaboration, "Geant4: A Simulation Toolkit", *Nucl. Instrum. and Methods A* **506** (2003) 250, doi:10.1016/S0168-9002(03)01368-8.

[32] O. Djuvsland and J. Nystrand, "Single and Double Photonuclear Excitations in Pb+Pb Collisions at $\sqrt{s_{NN}}$ = 2.76 TeV at the CERN Large Hadron Collider", *Phys. Rev. C* **83** (2011) 041901, doi:10.1103/PhysRevC.83.041901, arXiv:1011.4908.

[33] I. P. Lokhtin and A. M. Snigirev, "A model of jet quenching in ultrarelativistic heavy ion collisions and high-p_{T} hadron spectra at RHIC", *Eur. Phys. J. C* **45** (2006) 211, doi:10.1140/epjc/s2005-02426-3, arXiv:hep-ph/0506189.

[34] CMS Collaboration, "Observation of Long-Range Near-Side Angular Correlations in Proton-Proton Collisions at the LHC", *JHEP* **09** (2010) 091, doi:10.1007/JHEP09(2010)091, arXiv:1009.4122.

[35] CMS Collaboration, "Long-range and short-range dihadron angular correlations in central PbPb collisions at a nucleon-nucleon center of mass energy of 2.76 TeV", *JHEP* **07** (2011) 076, doi:10.1007/JHEP07(2011)076, arXiv:1105.2438.

[36] CMS Collaboration, "Observation of long-range near-side angular correlations in proton-lead collisions at the LHC", *Phys. Lett. B* **718** (2013) 795, doi:10.1016/j.physletb.2012.11.025, arXiv:1210.5482.

[37] CMS Collaboration, "Multiplicity and transverse momentum dependence of two- and four-particle correlations in pPb and PbPb collisions", *Phys. Lett. B* **724** (2013) 213, doi:10.1016/j.physletb.2013.06.028, arXiv:1305.0609.

[38] B. H. Alver, C. Gombeaud, M. Luzum, and J.-Y. Ollitrault, "Triangular flow in hydrodynamics and transport theory", *Phys. Rev. C* **82** (2010) 034913, doi:10.1103/PhysRevC.82.034913, arXiv:1007.5469.

[39] N. Borghini and J.-Y. Ollitrault, "Momentum spectra, anisotropic flow, and ideal fluids", *Phys. Lett. B* **642** (2006) 227, doi:10.1016/j.physletb.2006.09.062, arXiv:nucl-th/0506045.

[40] M. L. Miller, K. Reygers, S. J. Sanders, and P. Steinberg, "Glauber modeling in high energy nuclear collisions", *Ann. Rev. Nucl. Part. Sci.* **57** (2007) 205, doi:10.1146/annurev.nucl.57.090506.123020, arXiv:nucl-ex/0701025.

[41] B. Alver, M. Baker, C. Loizides, and P. Steinberg, "The PHOBOS Glauber Monte Carlo", (2008). arXiv:0805.4411.

[42] H.-J. Drescher, A. Dumitru, A. Hayashigaki, and Y. Nara, "The eccentricity in heavy-ion collisions from color glass condensate initial conditions", *Phys. Rev. C* **74** (2006) 044905, doi:10.1103/PhysRevC.74.044905, arXiv:nucl-th/0605012.